SANDIA REPORT
SAND2013-10104
Unlimited Release
December 2013

Exploring Graphene Field Effect Transistor Devices to Improve Spectral Resolution of Semiconductor Radiation Detectors

Richard K. Harrison, Stephen W. Howell, Jeffrey B. Martin, Allister B. Hamilton

Prepared by
Sandia National Laboratories
Albuquerque, New Mexico 87185 and Livermore, California 94550

Sandia National Laboratories is a multi-program laboratory managed and operated by Sandia Corporation, a wholly owned subsidiary of Lockheed Martin Corporation, for the U.S. Department of Energy's National Nuclear Security Administration under contract DE-AC04-94AL85000.

Approved for public release; further dissemination unlimited.

Sandia National Laboratories

Issued by Sandia National Laboratories, operated for the United States Department of Energy by Sandia Corporation.

NOTICE: This report was prepared as an account of work sponsored by an agency of the United States Government. Neither the United States Government, nor any agency thereof, nor any of their employees, nor any of their contractors, subcontractors, or their employees, make any warranty, express or implied, or assume any legal liability or responsibility for the accuracy, completeness, or usefulness of any information, apparatus, product, or process disclosed, or represent that its use would not infringe privately owned rights. Reference herein to any specific commercial product, process, or service by trade name, trademark, manufacturer, or otherwise, does not necessarily constitute or imply its endorsement, recommendation, or favoring by the United States Government, any agency thereof, or any of their contractors or subcontractors. The views and opinions expressed herein do not necessarily state or reflect those of the United States Government, any agency thereof, or any of their contractors.

Printed in the United States of America. This report has been reproduced directly from the best available copy.

Available to DOE and DOE contractors from
U.S. Department of Energy
Office of Scientific and Technical Information
P.O. Box 62
Oak Ridge, TN 37831

Telephone: (865) 576-8401
Facsimile: (865) 576-5728
E-Mail: reports@adonis.osti.gov
Online ordering: http://www.osti.gov/bridge

Available to the public from
U.S. Department of Commerce
National Technical Information Service
5285 Port Royal Rd.
Springfield, VA 22161

Telephone: (800) 553-6847
Facsimile: (703) 605-6900
E-Mail: orders@ntis.fedworld.gov
Online order: http://www.ntis.gov/help/ordermethods.asp?loc=7-4-0#online

Issued by Sandia National Laboratories, operated for the United States Department of Energy by Sandia Corporation.

SAND2013-10104
Unlimited Release
December 2013

Exploring Graphene Field Effect Transistor Devices to Improve Spectral Resolution of Semiconductor Radiation Detectors

Richard K. Harrison[a], Stephen W. Howell[b], Jeffrey B. Martin[a], Allister B. Hamilton[b]

[a]Nuclear Forensics R&D Department, [b]Rad Hard CMOS Technology Department
Sandia National Laboratories
P.O. Box 5800, MS0968
Albuquerque, New Mexico 87185-0968

Abstract

Graphene, a planar, atomically thin form of carbon, has unique electrical and material properties that could enable new high performance semiconductor devices. Graphene could be of specific interest in the development of room-temperature, high-resolution semiconductor radiation spectrometers. Incorporating graphene into a field-effect transistor architecture could provide an extremely high sensitivity readout mechanism for sensing charge carriers in a semiconductor detector, thus enabling the fabrication of a sensitive radiation sensor. In addition, the field effect transistor architecture allows us to sense only a single charge carrier type, such as electrons. This is an advantage for room-temperature semiconductor radiation detectors, which often suffer from significant hole trapping. Here we report on initial efforts towards device fabrication and proof-of-concept testing. This work investigates the use of graphene transferred onto silicon and silicon carbide, and the response of these fabricated graphene field effect transistor devices to stimuli such as light and alpha radiation.

ACKNOWLEDGMENTS

The authors would like to thank the Defense Systems and Assessments Investment Committee for their support.

CONTENTS

1. Introduction 6

2. Experimental Methods 9
   2.1 Operating Principles of a Graphene Device 9
      2.1.1 Basic GFET Operation Principles 9
      2.1.2 Hybrid Radiation Detector Based on a Charge Sensing GFET 10
   2.2 Device Fabrication 11

3. Results 13
   3.1 Detection and Analysis of Optically Generated Charges 13
   3.2 Detection and Analysis of Alpha Radiation with a GFET Device 16

4. Conclusions 20

5. References 21

Distribution 22

FIGURES

Figure 1: Dramatic change in the resistance of graphene with applied voltage. 9
Figure 2: Schematics of a GFET device. 10
Figure 3: Hybrid GFET detector schematic and operating principle. 10
Figure 4: A labeled micrograph of a characteristic GFET device. 11
Figure 5: Optical detection using a GFET device. 13
Figure 6: Effect of back-gate voltage on the GFET optical response. 14
Figure 7: Temporal dependence of current change as a function of the applied voltage. 14
Figure 8: The effect of charge buildup beneath a GFET device near the Dirac point. 15
Figure 8: Analysis of the radiation resistance of the GFET devices. 16
Figure 9: Detection of alpha particles from a Po-210 source using top-side irradiation. 17
Figure 10: Repeatability of alpha radiation detection. 17
Figure 11: Parameter variation in GFET alpha detection. 18
Figure 12: Statistical analysis of the sample-to-sample variation in the detected signal from alpha radiation. 19

TABLES

Table 1. Semiconductor Material Properties for Radiation Detection 7

1. INTRODUCTION

A high-resolution radiation spectrometer capable of distinguishing narrowly-separated energy peaks at, or near, room temperature would provide a new capability for radiation detection and measurement in fields ranging from materials characterization and astrophysics to homeland security and nuclear forensics. The accurate detection of high energy MeV-level gamma rays is of crucial importance for identifying the isotopic or nuclear interaction source of the radiation. Along with detection efficiency, energy resolution is the key attribute for a radiation spectrometer. The full-width half-max (FWHM) energy resolution of a given detector is dominated by three terms: the statistical fluctuation of charge carrier generation, the effect of incomplete charge carrier collection, and the electrical noise of the system dominated by the detector capacitance. Improved detector resolution allows for low count peak identification, reduced spectral overlap, and higher confidence in estimating source strength. The current challenge in radiation spectrometry is that the highest resolution can only be achieved with high-purity germanium (HPGe) detectors cooled to liquid nitrogen temperatures (77 K). The low temperature is needed to 'freeze out' thermally generated charge carriers that are generated because of the low bandgap of germanium (0.67 eV). This necessitates the use of large liquid nitrogen dewars and constant refilling to maintain the temperature, which limits mobile use and the number of detectors utilized. Germanium is the most widely used semiconductor detector material because of the large crystal sizes that can be achieved on account of the large depletion depth in highly purified material, which allows for high-energy gamma rays to be completely absorbed in the detector volume. Typical HPGe detectors FWHM resolutions of 3.3% for low energy photons (5.9 keV) and 1.3% for higher energy gamma rays (1.33 MeV)[1].

Lechner *et al.* achieved notable energy resolutions using a drift detector configuration on a silicon substrate[2]. The primary advantage of a drift-type detector is that charges can be 'focused' and collected at an on-chip charge detector with much lower capacitance and corresponding electrical noise contribution to improve energy resolution. These devices can also be fully depleted, indicating that charges can be efficiently collected from throughout the volume of the detector. Silicon also has a larger bandgap (1.1 eV) than germanium, reducing the magnitude of thermal charge carrier generation. Furthermore, the vast experience with silicon substrates in the microchip industry has enabled the fabrication of advanced architectures for silicon drift detectors. With a ring-configuration set of electrodes feeding an on-chip junction field-effect transistor charge collector and amplifier, Lechner *et al.* achieved full-width half-max values of 3.8%, 2.9% and 2.4% at temperatures of 300 K, 263 K and 200 K, respectively, for 5.9 keV photons. The temperatures at which these remarkable energy resolutions were obtained can now be reached with solid-state thermoelectric Peltier cooling systems, which are much more portable and operationally useful than liquid nitrogen dewars for field testing. However, silicon detectors are limited to the detection of low-energy photons, as the techniques for purifying germanium can achieve lower impurity levels than can be obtained in silicon. Higher purity materials lead to larger volume detectors through the increased depletion depths, and correspondingly lower losses due to incomplete radiation energy deposition. Furthermore, silicon is a low-density, low-Z (atomic number) material, which further reduces the interaction probability for high-energy gamma rays. Thus, there is a strong impetus towards being able to use advanced configurations in a detector where high-energy gammas could also be detected.

Several other semiconductor materials have also been identified as potential candidates for gamma ray detectors, including the high-density, high-Z materials mercury iodide (HgI_2) and cadmium zinc telluride (CdZnTe or CZT). While these materials have very good energy deposition behavior and can be fabricated in large volumes, their electrical and charge collection properties suffer in relation to silicon and germanium crystals. Additionally, the techniques and technologies for doping, processing and integrating circuits for these wide-band compound semiconductors are much less advanced than for elemental semiconductors. One specific issue with HgI_2 and CZT are the large differences between the electron and hole mobilities and related lifetimes, which can limit the charge collection efficiency in standard collection configurations. Table 1 shows the measured electrical properties and material constants for several semiconductor materials of interest.

Table 1. Semiconductor Material Properties for Radiation Detection

Material	Density (g/cm^3)	Bandgap (eV)	Electron Mobility ($cm^2/V{\cdot}s$)	Hole Mobility ($cm^2/V{\cdot}s$)	Mobility Ratio
Silicon (Si)	2.33*	1.12*	1900†	500†	3.8
Silicon Carbide (6H SiC)	3.21*	2.86‡	400‡	75‡	5.3
Germanium (Ge)	5.33*	0.67*	3800†	1820†	2.1
Mercury Iodide (HgI_2)	6.4*	2.13*	100§	4§	25
Cadmium Zinc Telluride ($Cd_{0.8}Zn_{0.2}Te$)	6.0*	1.64*	1350*	120*	11.3

*Knoll[1] †Haynes[3] ‡Hudgins *et al.*[4] §Minder *et al.*[5]

The challenges of charge collection in materials with large electron-hole mobility ratios are significant, but detector performance can be improved in these cases through the use of single polarity charge sensing configurations, where only the electrons are detected. Luke[6] and He *et al.*[7] used coplanar grid electrode readout electronics on a CZT substrate to effectively mitigate the problem of incomplete hole collection. More recently, Abbene *et al.*[7] demonstrated 1.9% FWHM peak resolution on a 59.5 keV photon using a unipolar, multiple electrode approach on a CZT substrate at 263 K. Further resolution gains could potentially be obtained with a reduction in the system readout capacitance, as Luke, et al., discuss in a subsequent paper[8]. Here, we investigate the potential of an on-chip graphene field-effect transistor (GFET) for unipolar charge sensing in radiation spectrometry applications.

Graphene, a planar, atomically thin form of carbon, has unique electrical and material properties, including very high mechanical strength, extremely high ambipolar mobilities and high thermal conductivity. Graphene can also be patterned using standard microchip fabrication processes. Graphene could be of specific interest in the development of a room-temperature high resolution semiconductor radiation spectrometer because of its almost negligible intrinsic capacitance[9]. Incorporating graphene into a field-effect transistor architecture could provide an

extremely high sensitivity readout mechanism with on chip amplification for sensing charge carriers in a semiconductor detector, thus potentially enabling the fabrication of a sensitive radiation sensor with very high resolution. Most relevantly, graphene has recently been demonstrated to be transferrable to any arbitrary substrate material[10]. In this report, we discuss initial proof-of-concept experiments towards the use of a GFET as charge sensor for radiation spectrometry.

2. EXPERIMENTAL METHODS

2.1 Operating Principles of a Graphene Device

Among the set of extraordinary properties of graphene, one of the arguably most interesting is the exceptional electrical transport behavior. Graphene can be thought of as a unique zero-bandgap semiconductor (semimetal) where the cones of the valence band and conduction band meet at the Dirac point (point where the film is charge neutral). Graphene energy dispersion is conical (semimetal), unlike other traditional semiconductors where the dispersion is more parabolic. This property is extraordinary because it is responsible for the long-range ballistic transport and corresponding extremely high charge carrier mobilities. Graphene's behavior is also interesting because large modification in carrier density and type can be obtained by moving the Fermi level within the film using an applied transverse electric field. Figure 1, taken from Geim and Novoselov[11], illustrates this point.

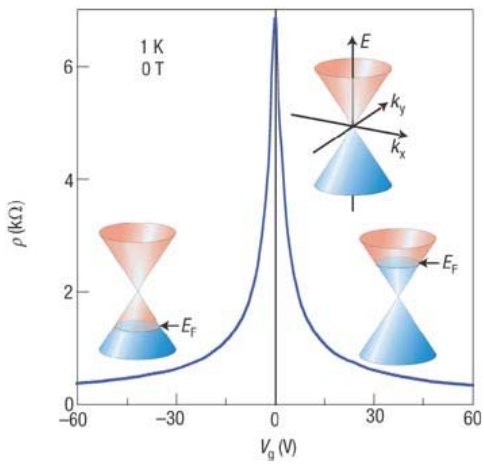

Figure 1: Dramatic change in the resistance of graphene with applied voltage.

2.1.1 Basic GFET Operation Principles

Any electric field applied to the graphene will affect the conductivity by shifting the Fermi level from a *p*-type material at negative voltages to an *n*-type material at positive voltages. The collection of charges beneath the insulator layer, whether electrons or holes, will exert an electric field effect that can change the conductivity. Due to these extraordinary charge transfer properties, graphene has been the subject of great interest for replacing or augmenting silicon microelectronic technologies with improved speed and efficiency. The dramatic sharp feature in the graphene current vs. voltage response has recently been utilized to create GFET devices, one of the basic microelectronic circuit building blocks. Fundamentally, field effect transistors work by controlling a perpendicular electronic flow with small applied voltage. Figure 2 shows a GFET device fabricated during a three year, Sandia-funded project aimed at enabling graphene nanoelectronics.

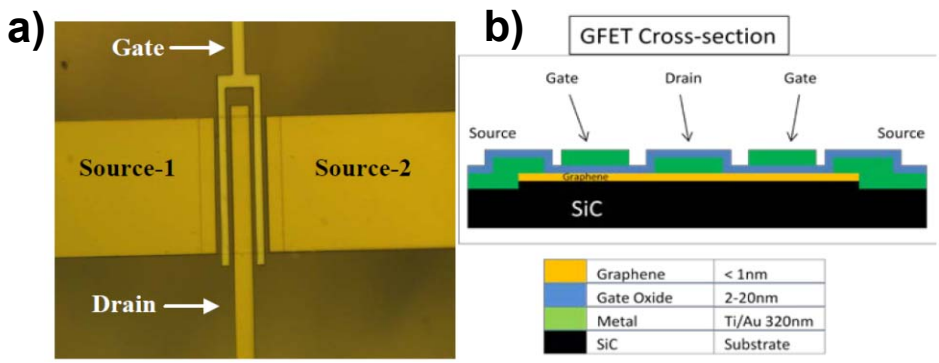

Figure 2: Schematics of a GFET device. a) Optical top-down image of a GFET with labeled electrodes. b) Profile schematic of graphene device structure.

2.1.2 Hybrid Radiation Detector Based on a Charge Sensing GFET

To develop novel radiation detectors, we fabricate a GFET on top of a semiconductor absorber. Figure 3 is a schematic of our device (similar to devices reported by Yong Chen group at Purdue University[12]). The GFET is electrically isolated from the absorber by a thin insulator, which acts as a gate dielectric.

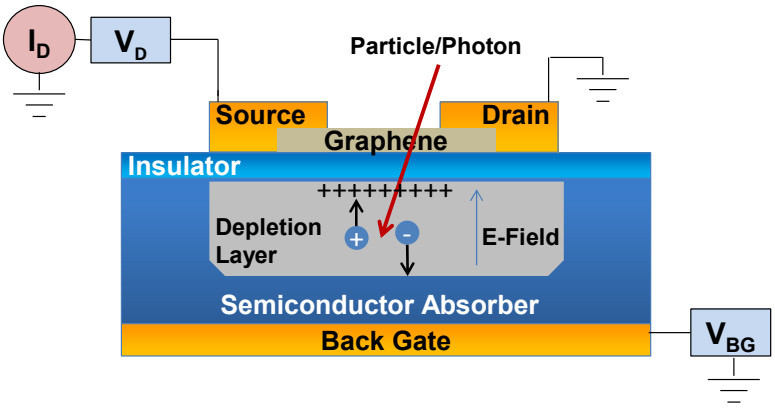

Figure 3: Hybrid GFET detector schematic and operating principle.

This device geometry is analogous to a metal-oxide-semiconductor (MOS) junction. When a voltage is applied to the semiconductor, via a backside ohmic contact, a depletion region forms underneath the graphene in the semiconductor. In the depletion region, the remaining fixed charge (dopant) creates an internal electric field that will separate electron-hole pairs generated by an energetic event. Separated charge then collects at the insulator/semiconductor interface, which enhances the transverse electric field being applied to the graphene. By applying a constant source-to-drain voltage, shifts in the graphene conductivity can be measured as changes in source-drain current.

The depth of the depletion region determines the number of electron/holes pairs that will be collected and is related to the dopant density, as well as the magnitude of the back-gate voltage.

2.2 Device Fabrication

Graphene Field Effect Transistor (GFET) devices were fabricated in a multistep process using a combination of wet chemistry transfer and lithographic definition procedures. The devices were fabricated on two different substrates: low-doped, 5 kΩ·cm resistivity, n-type silicon (Si) or vanadium counter-doped, semi-insulating silicon carbide. It is important to use substrates with low dopant concentrations in detector applications to reduce charge carrier recombination. The GFET device fabrication procedure was largely the same for either substrate material. The substrates were diced to a 1 cm^2 square. First, a metal back electrode consisting of a 100 nm gold contact was deposited on a 10 nm titanium adhesion layer. For some samples, an ohmic contact was fabricated at the back electrode using ion implantation. Next, an insulating layer was deposited on the substrate top surface using plasma-enhanced chemical vapor deposition (PE-CVD). This insulator was either silicon dioxide with a 100 nm thickness or silicon nitride with a 50 nm thickness. After this insulator deposition, single layer graphene (Trivial Transfer, ACS Material LLC.) was transferred onto the substrates from a polymer support. In this process, the graphene could be floated off of the polymer support and attached to a new substrate through immersion in water. Subsequently, a PMMA backing layer on the graphene could be dissolved using acetone.

After the graphene was attached to the semiconductor, arrays of GFET devices were defined using a custom-design lithographic mask to first define the graphene transistor layer (device-to-device isolation), and then to fabricate metal contacts for the source and drain electrodes. These metal electrodes consisted of 100 nm of gold on a 10 nm titanium adhesion layer. Two different GFET device arrays were fabricated on the substrates to examine the effect of device area on performance: smaller 250 × 100 µm devices with 100 µm electrode pads and larger 450 × 200 µm devices with 200 µm electrode pads. Figure 4 shows a schematic and image of the device structure.

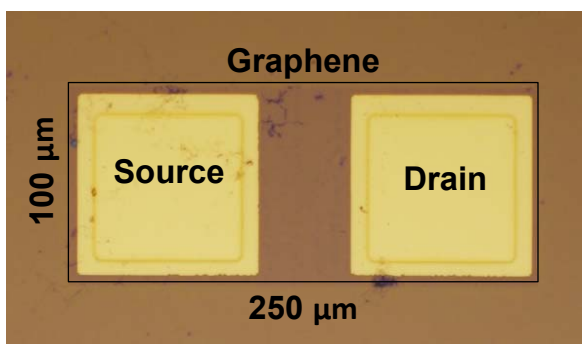

Figure 4: A labeled micrograph of a characteristic GFET device.

After fabrication, optical and electrical inspections were first used to verify that the GFET devices were well-defined and functional. As a custom, low-throughput device, it is essential to ensure that each GFET device responds as expected to applied electrical stimuli. Specifically, each device was tested for linearity in the current response to a voltage applied across the source and drain terminals. Microscopy was also used to verify coverage of the transferred graphene over the GFET device arrays.

All testing was performed using a probe station (Signatone) emplaced within an isolation chamber to minimize vibration and noise. The back gate voltage was applied directly to the back

metal contact on the substrate. The source and drain voltages were applied to the individual electrodes corresponding to a single defined GFET device using a microscope-guided micropositioner probes. A typical source-to-drain bias potential was 0.1 V, although this could be held at any voltage relative to the back gate to probe the effect of collecting electron and hole charge carriers beneath the insulator on the graphene conductivity.

Optical measurements were taken using either a halogen (Schott Modulamp with EKE bulb) or metal halide (EXFO X-Cite 120) lamp. The halogen lamp emits mainly in the 390 – 740 nm range, while the metal halide lamp emits strongly down to 300 nm. The short wavelengths accessible with the metal halide lamp were used to test the devices with a wide bandgap SiC substrate. In either case, the optical light was passes through a beam guide and focused onto the GFET device using a microscope objective. An advantage of this configuration was that the light could be turned on and off from outside the isolation chamber with negligible vibration or other impact to the test setup.

Radiation sensor development tests were performed with a polonium-210 (Po-210) alpha emitter, normally sold as a static eliminator (NRD Static Control 1U400). The alpha emitter was selected because of the confined radiation fields and localized energy deposition available with this source, which had a relatively high initial activity of 500 microcuries (μCi). We estimate that alpha particles incident from this source at an in-air distance of 1 cm have a range in silicon of 18 μm. Choosing a radiation source that is not an external safety hazard allowed considerable flexibility in testing, and the source activity and energy deposition for a small region very near the source surface exceeds what might be available in high radiation areas. The alpha source was mounted on a pneumatic, low vibration cantilevered piston that could be inserted to irradiate the mounted GFET devices. The piston was controlled from outside the isolation chamber to minimize system noise.

3. RESULTS

3.1 Detection and Analysis of Optically Generated Charges

We first probed the optical response of the GFET devices to examine the detector performance. These tests provide a direct measure of the ability of the device to collect charge and then measure its accumulation beneath the insulator through an effect on the graphene conductivity. We performed a set of experiments on the optical response using several GFET devices on three different substrates and using two different light sources with different filters. These experiments allowed us to test a wide range of conditions while minimizing the hazard of working directly with the radiation source.

The first test, shown in Figure 5, shows the response of the GFET device on a silicon carbide substrate to light from the halogen lamp. No response was observed with or without the incident light when no back gate voltage was applied. With an applied back gate voltage (Vbg), we observe a stabilization time of approximately 40 seconds, which we attributed to mild charge buildup at or near the semiconductor-insulator interface. Some variation was observed between the final stabilization current resulting from a slight hysteresis effect, but this minor effect could potentially be overcome by reverse biasing the device. The net current change is a more important indicator of the overall detector performance. As shown in the 'Light On' case of Figure 5, we observe a strong detector response to optical light. This is shown as a 17.6 µA drop in the current flow over the 40 seconds of optical illumination, representing a 50.3 % change on the stabilized initial value. Interestingly, the drop was not linear, but rather asymptotic. This suggests competing mechanisms of charge buildup and electrostatic repulsion or diffusion that result in an eventual equilibrium for a given charge generation rate. After the light was extinguished, there is a gradual return toward the initial signal level.

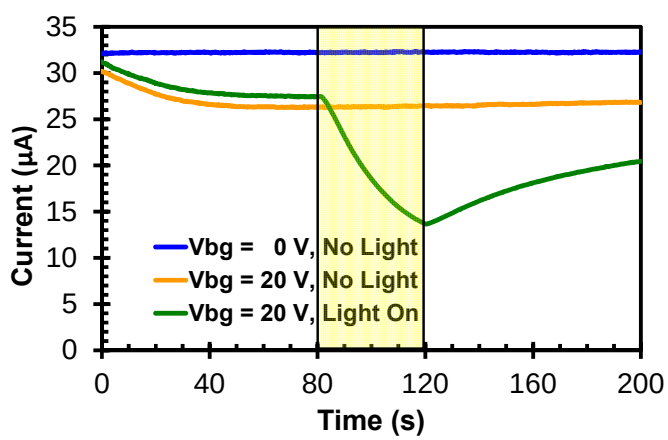

Figure 5: Optical detection using a GFET device.

As a follow-up test, we next examined the effect of the back gate voltage on the GFET optical response. Figure 6 presents the results of these experiments. We also noticed that the response is quite different for the case of a positive voltage differential (from the back gate to the source and drain levels) where holes would collect under the insulator surface, which resulted in a current drop across the graphene transistor as in the case of a negative differential where electrons would

collect at the GFET device, which resulted in a current gain. We also observe that the rate of current change increases with the applied potential difference. For small applied voltages or at short illumination times, the current change during optical illumination has a linear trend, but at higher voltages, the current asymptotically approaches a set value which we hypothesize is caused by charge carrier repulsion.

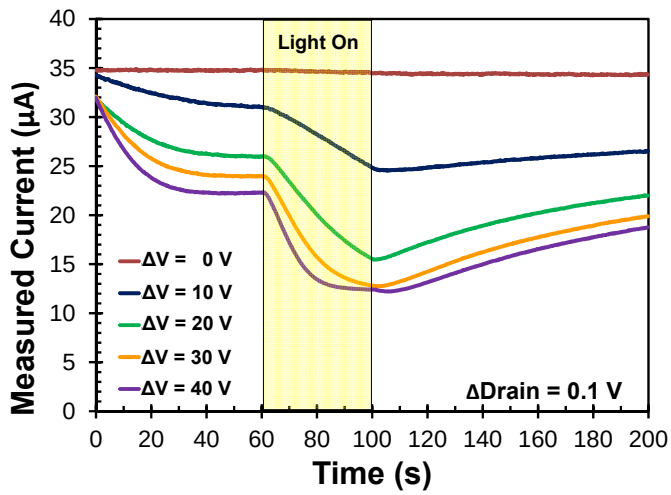

Figure 6: Effect of back-gate voltage on the GFET optical response.

We then extracted data out of some repeated runs under these conditions. Given the signal saturation, we primarily consider the initial slope or rate of current change with time for the first few seconds of the optical exposure. A plot showing some of the normalized line profiles is shown in Figure 7. The initial slope on the current versus time changes proportionally with the applied voltage for these measurements. This data can provide an indication on the achievable sensitivity of these devices.

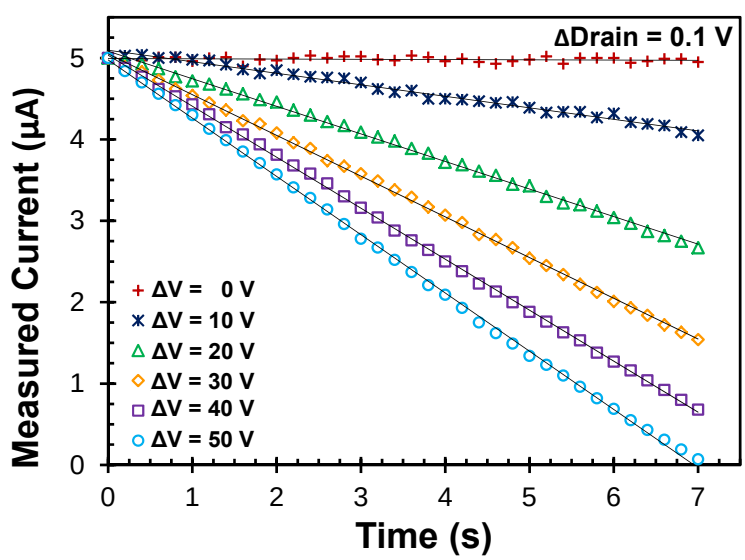

Figure 7: Temporal dependence of current change as a function of the applied voltage.

Finally, we investigated the behavior of the GFET junction as it relates to charge transfer near the charge neutral point for a GFET fabricated on a high-quality low-doped silicon substrate. Consistent with our hypothesis that charge builds up beneath the graphene surface, the charge can create an effect similar to a change in the back gate voltage. Interestingly, this buildup can exhibit an exotic effect in the current flow if the charge neutral point is crossed. Figure 8 shows several examples illustrating this intriguing phenomenon.

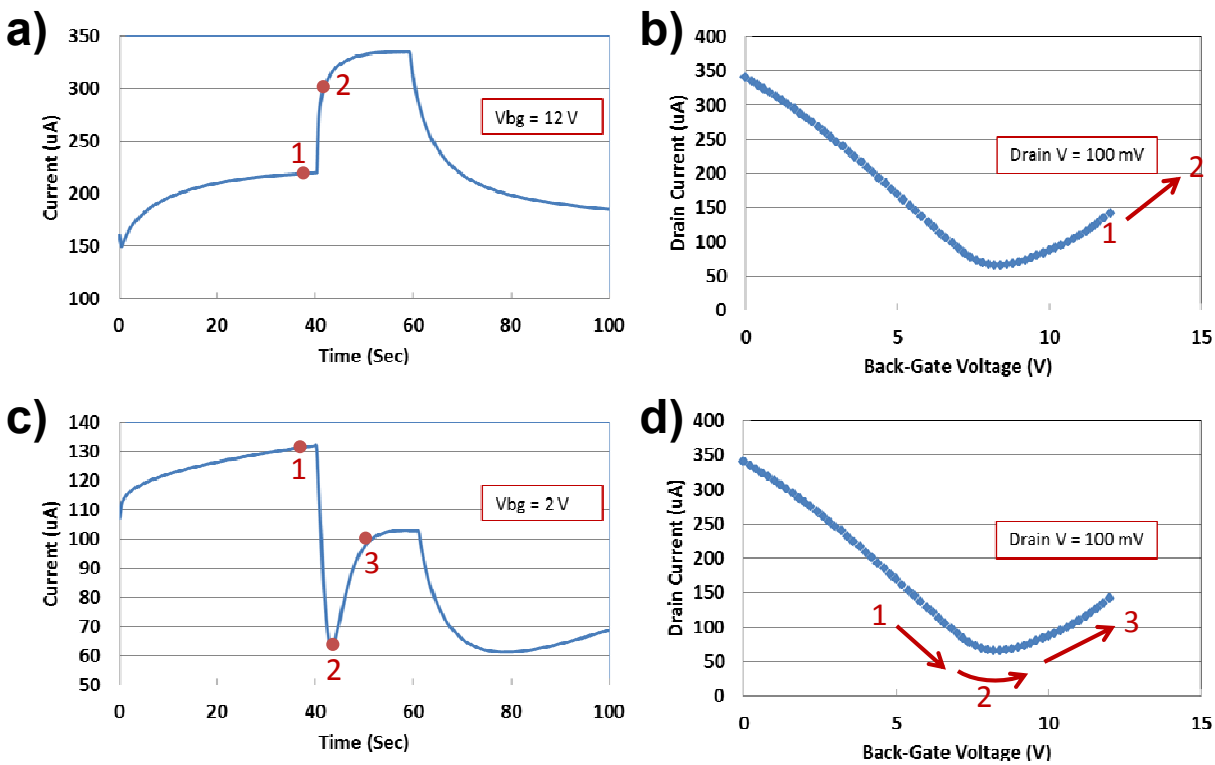

Figure 8: The effect of charge buildup beneath a GFET device near the Dirac point. a) Current versus time for a 12 V applied back-gate voltage. b) Location of these points on the current versus voltage map of the charge neutrality location. c) Current versus time for a 2 V applied back-gate voltage. d) Crossing over the charge neutrality point leads to a change in the primary current carrier and a reversal in the current change with time.

Interestingly, if the initial voltage is close to the charge neutrality point and enough charges build up to cross the threshold, a dramatically sharp reversal in the charge versus time trend occurs. This sharp response could potentially be employed to create an extremely sensitive threshold dependent charge detector.

Even without employing this technique, we find that these initial, unoptimized prototype GFET devices are surprisingly sensitive to incident light, even without amplification. The broadband halogen light source delivers an irradiance of 4.5 mW/cm^2 to the test setup with an estimated average photon energy of 2 eV (640 nm). However, only 4 μW of this energy is incident on GFET device, and 35% of this light would be reflected at the silicon interface. Even assuming that the GFET device could collect generated charge carriers from an area 80 times as

large as the device itself without any guide electrodes, the net signal sensitivity would still be ~0.5 A/W, which is comparable to commercial silicon photodiodes.

3.2 Detection and Analysis of Alpha Radiation with a GFET Device

Our initial radiation tests were designed with a backside alpha irradiation in mind. However, these tests were unsuccessful, leading us to consider alternative configurations and to try to understand why the tests failed. Upon further analysis, we identified a probable scenario where the device acts like a metal-oxide-semiconductor capacitor-type junction and the depletion region does not penetrate the full depth of the device. If this is correct, it means that charge carriers generated near the back surface would not 'feel' the applied voltage and that the fields would be confined to the region near the top surface of the detector. With this hypothesis of limited depletion depth in mind, we then considered front side irradiation. Before this was attempted, however, we first examined the possibility of radiation-induced damage occurring to the graphene sheet due to alpha impacts. To quantify this possibility, we examined the graphene resistance as a function of radiation time for five different GFET devices on a silicon substrate. Each of these devices was subjected to a 300 second alpha radiation exposure with the source position to maximize dose to the device. Figure 9 presents the change in resistance for the before and after exposure cases. The minor changes in resistance for the exposed GFET devices imply that the radiation caused little damage to the devices. The changes could also result from changes in the probe contacts. Heavy charged particles, such as alphas, represent a 'worst-case' scenario for potential damage to a graphene layer, but the slight changes observed here indicate that other radiation sources like x-rays and gammas, should have limited effect on device operation.

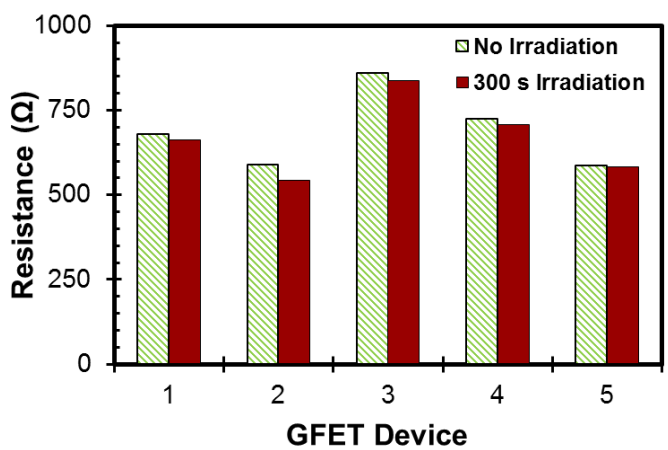

Figure 9: Analysis of the radiation resistance of the GFET devices.

Subsequently, we directly tested the effect of alpha irradiation on a GFET device built on SiC to determine if this configuration could be used to detect ionizing radiation. Figure 10 presents the significant changes in the current when the radiation source was present. Here we observe a jagged curve resulting from charges generated by individual alpha particles interacting with the silicon carbide substrates, analogous to drops of rain in comparison with the river of charges generated by the optical illumination.

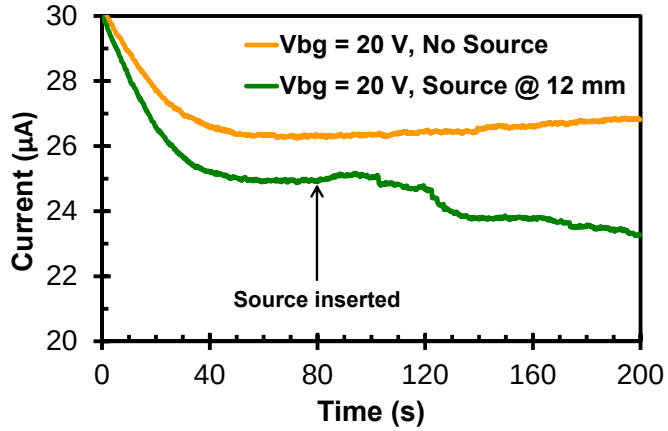

Figure 10: Detection of alpha particles from a Po-210 source using top-side irradiation.

The charge-sensing tests using the alpha source were characterized by sharp point-to-point drops in the current, which we conclude come from alphas that deposit a large amount of energy in the sensitive region of the detector. Figure 11 shows that the overall slope of the current change with time was similar for three different exposures, but the statistically random interaction at any given time could lead to larger or smaller changes.

While the observed radioactive signal changes are modest in comparison to what was observed during optical illumination, we note that the net energy deposition for the same area is more than three orders of magnitude greater for the optical illumination than for the alpha particles with our 250 µCi Po-210 source at a distance of 1 cm. Furthermore, much of the optical energy deposition will occur very near to the semiconductor-insulator interface, while the alpha energy deposition will occur throughout the range of the particles in the semiconductor material.

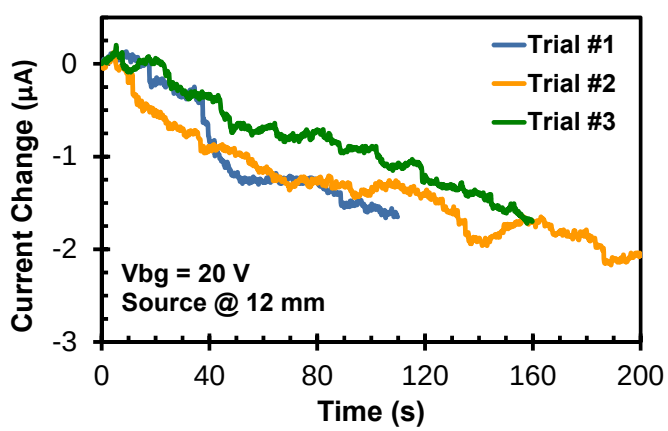

Figure 11: Repeatability of alpha radiation detection.

We next varied the radiation and detection conditions to examine their effects. Figure 12a shows that the effect of changing the alpha source to GFET detector distance accounted for a difference in the current drop of approximately a factor of two, with changes of 0.82 and 1.68 µA for the 25 mm and 12 mm separations, respectively. This might be expected to be an even larger difference as both the number of alphas and the average energy would be larger for the 12 mm separation. We estimate that the average alpha energy would be 1.1 MeV for the 25 mm separation and 2.9

MeV for the 12 mm distance. Additionally, we modeled the random alpha emission from the source with these detector configurations and found that twice as many alpha particles are incident on the GFET detector for the near (12 mm) and far source (25 mm) configurations in this planar-type geometry. However, for most of the alpha range, the energy deposited per unit distance changes only weakly with alpha energy[1]. We also hypothesize that the depletion width in the SiC substrate is smaller than the range of alphas in the material, implying that only a relatively small fraction of the total deposited alpha energy contributes to the detected signal. Thus, even though the alpha energy is much greater in the short range case, it is conceivable that a similar number of charge carriers might be detected per alpha in both cases.

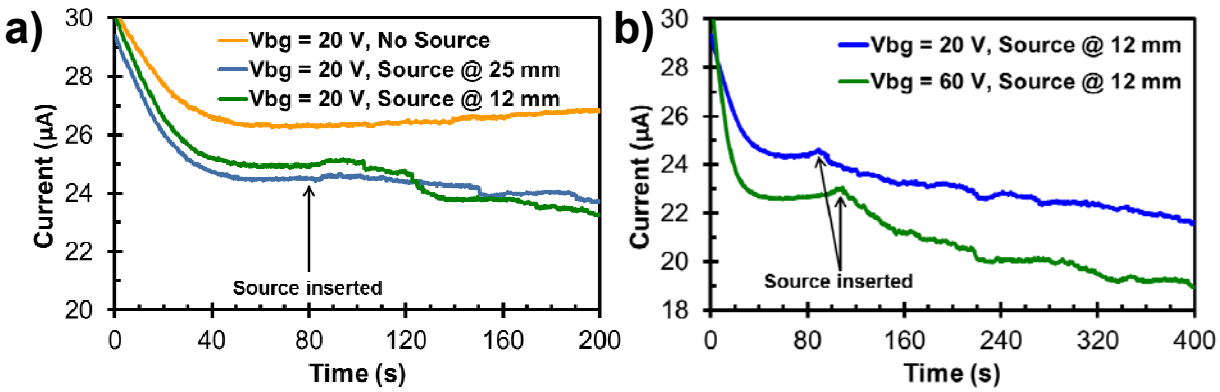

Figure 12: Parameter variation in GFET alpha detection. a) Change in source distance. b) Change in back-gate voltage.

Figure 12b shows that the back-gate voltage does have a significant effect on the detected signal. In this case, we observe a much larger rate of current change over the two tests for the case of V_{bg} = 60 V versus V_{bg} = 20 V. Quantitatively, these changes were 2.36 μA (10.2%) and 1.52 μA (6.2%), respectively. This difference is one indication that the effective region of charge collection expands at larger applied voltages, potentially both in depth and expanse.

It is perhaps more informative to statistically analyze the changes between each time step in the GFET current to consider the potential of using this device as a radiation spectrometer. In this case, the signal drop in a given short amount of time could be related to the energy deposition by individual alpha particles. In this case, our sensitivity is relatively low, as we expect over 400 alpha particles to interact with the GFET area per time period measured, but this could provide a path forward towards radiation spectrometry. Here we divide the sample-to-sample change in the current into 25 nA bins and plot the frequency of each shift, shown in Figure 13a. We also examine the maximum value of the sample-to-sample variations in the current for the control and irradiation conditions (Figure 13b). Here, we see that the current change frequency is shifted and has a longer tail in the irradiation cases. We also observe that the sample-to-sample changes are not dramatically different between the 20 and 60 V back gate conditions, which may imply that the energy deposited is similar per alpha interaction, but longer exposures may be necessary to say this conclusively. We also note that the maximum current gains are small and similar for all four cases shown in Figure 13b, consistent with random noise, but that the current drops are significantly larger for the alpha irradiation conditions, indicative of specific charge-carrier generation events.

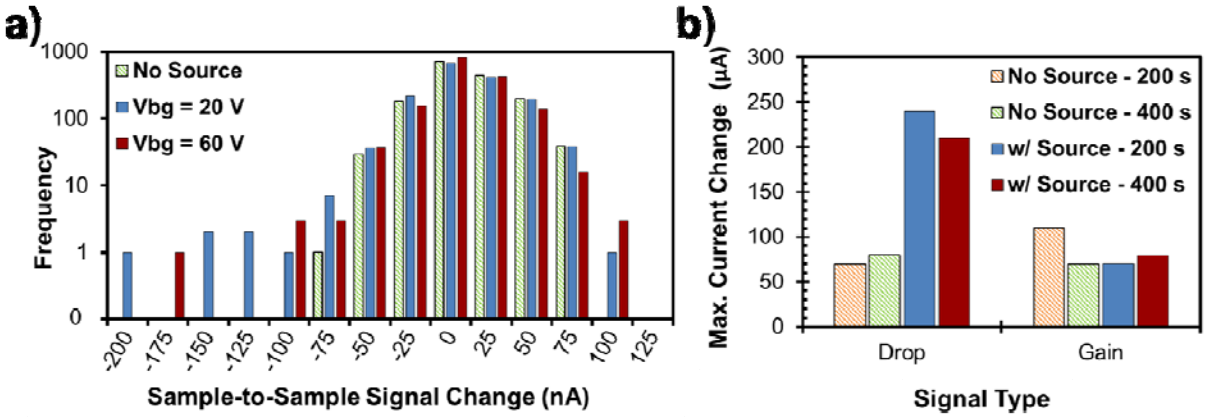

Figure 13: Statistical analysis of the sample-to-sample variation in the detected signal from alpha radiation. a) Log-scale frequency analysis of the signal change for control, 20 V and 60 V cases. b) Maximum signal change over two points for source measurement.

4. CONCLUSIONS

Here we have demonstrated the use of a GFET device to collect optical photon and radiation-induced charges in a semiconductor detector. We showed that the graphene could be transferred onto multiple different semiconductor substrates and that functioning GFET devices could be fabricated from these deposited layers. Furthermore, we found that we could detect the presence of optical- and radiation-generated charge carriers in the semiconductor material through the variation of the voltage-dependent current flow across the GFET device. In the course of this project, we have developed an understanding of the device physics for a MOS-like charge-sensitive GFET device. Specifically, we find that the depletion width is a dominant factor for charge generation and collection, and that the unique nature of the charge neutrality point in graphene causes distinctive effects that can be used for optical and radiation detection.

The graphene was transferred to this device in a process that could be applied to a flat substrate of virtually any material, illustrating its utility for advanced compound semiconductor materials. Furthermore, the light and radiation detection technique demonstrated here makes use of one charge carrier, not carrier separation, and can thus make use of materials with a large discrepancy in the electron to hole mobilities that cannot be effectively employed in other situations. The experiments and analysis performed through this project demonstrate the potential utility of these devices, which recommend further study into the phenomena examined here.

5. REFERENCES

1. G.F. Knoll, Radiation Detection and Measurement, 3rd edition, John Wiley and Sons: Hoboken, NJ (2000).
2. P. Lechner *et al.* "Silicon drift detectors for high-resolution room temperature X-ray spectroscopy," *Nuclear Instruments and Methods in Physics Research A* **377**, 346-351 (1996).
3. W.M. Haynes, ed. CRC Handbook of Chemistry and Physics, 85th edition, CRC Press: Boca Raton, FL (2011).
4. J.L. Hudgins, G.S. Simin, E. Santi and M.A. Khan, "An Assessment of Wide Bandgap Semiconductors for Power Devices," *IEEE Transactions on Power Electronics* **18** (2003).
5. R. Minder, G. Majni, C. Canali, G. Ottaviani, R. Stuck, J.P. Ponpon, C. Schwab and P. Siffert, "Measurement of the drift velocity of charge carriers in mercuric iodide," *Journal of Applied Physics* **45**, 5074-5076 (1974).
6. P.N. Luke, "Unipolar Charge Sensing with Coplanar Electrodes – Application to Semiconductor Detectors," *IEEE Transactions on Nuclear Science* **42** (1995).
7. L. Abbene, S. Del Sordo, F. Fauci, G. Gerardi, A. La Manna, G. Raso, A. Cola, E. Perillo, A. Raulo, V. Gostilo and S. Stumbo, "Spectroscopic response of a CdZnTe multiple electrode detector," *Nuclear Instruments and Methods in Physics Research A* **583**, 324-331 (2007).
8. P.N. Luke, M. Ammon, and J.S. Lee, "Factors Affecting Energy Resolution of Coplanar-Grid CdZnTe Detectors," *IEEE Transactions on Nuclear Science* **51(3),** 1199-1203 (2004).
9. J. Xia, F. Chen, J. Li, and N. Tao, "Measurement of the quantum capacitance of graphene," *Nature Nanotechnology* **4**, 505-509 (2009).
10. J.W. Suk, A. Kitt, C.W. Magnuson, Y. Hao, S. Ahmed, J. An, A.K. Swan, B.B. Goldberg and R.S. Ruoff, "Transfer of CVD-Grown Monolayer Graphene onto Arbitrary Substrates," *ACS Nano* **5**, 6916-6924 (2011).
11. A.K. Geim and K.S. Novoselov, "The rise of graphene," *Nature Materials* **6**, 183-191 (2007).
12. A. Patil, G. Lopez, M. Foxe, I. Childres, C. Roecker, J. Boguski, I. Jovanovic and Y.P. Chen, "Graphene Field Effect Transistors for Detection of Ionizing Radiation," *IEEE Transactions* (2010).

DISTRIBUTION

1	MS0101	David R. Sandison	0110
1	MS0359	D. Chavez, LDRD Office	1911
1	MS0892	Stephen W. Howell	1748
1	MS0892	Allister B. Hamilton	1748
1	MS0968	Karen S. Rogers	5734
1	MS0968	Jeffrey B. Martin	5734
1	MS0968	Richard K. Harrison	5734
1	MS1078	Wahid L. Hermina	1710
1	MS1084	Richard Dondero	1748
1	MS1415	Frederick B. McCormick	1110
1	MS1415	Carlos Gutierrez	1114
1	MS0899	Technical Library	9536 (electronic copy)

Sandia National Laboratories